Rare Metal Materials and Engineering
Volume 49, Issue 1, January 2020
Available online at www.rmme.ac.cn

Science Press

Cite this article as: Rare Metal Materials and Engineering, 2020, 49(1): 0034-0041.

ARTICLE

Comparison of Electrical Ablation Properties Between Pantograph Materials: Ti_3AlC_2 and Cu-Ti_3AlC_2

Huang Xiaochen[1], Feng Yi[2], Qian Gang[2], Ge Jinlong[1], Zhang Xianfeng[1], Wang Chuanhu[1]

[1] Research Center of Silicon-based New Materials Engineering Technology, Bengbu College, Bengbu 233030, China; [2] Hefei University of Technology, Hefei 230009, China

Abstract: The electrical ablation properties of typical pantograph materials Ti_3AlC_2 as well as Cu-Ti_3AlC_2 were analyzed at 2, 5, 7 and 9 kV. The results show that the arc life of Cu-Ti_3AlC_2 is shorter than that of Ti_3AlC_2. The breakdown current shows the same condition. High speed camera was employed to record the arc morphologies of the two materials. The arc on Ti_3AlC_2 is more concentrated than that of Cu-Ti_3AlC_2, accompanied with more droplet splashes. The eroded surfaces of the two materials were observed by scanning electron microscopy (SEM). Compared to the eroded Cu-Ti_3AlC_2, Ti_3AlC_2 surface is more uneven, covered by "holes", "microcracks" and "splashes". The arc energy at different voltages was calculated. It shows that the arc energy of Cu-Ti_3AlC_2 material is less than that of Ti_3AlC_2 material at the same voltage. Raman spectrometer was used to determine the composition of the eroded surfaces. Summarizing the experimental results, it can be found that Cu-Ti_3AlC_2 is more suitable for pantograph material.

Key words: Ti_3AlC_2; Cu-Ti_3AlC_2; arc erosion; high speed camera

Since the opening of the world's first high-speed railway Shinkansen in Japan on October 1, 1964, the development of high-speed railway has gone through over 50 years of history. High-speed railway has the advantages of high safety, high speed, high punctuality, comfort and convenience, large capacity, less pollution and light energy consumption, which has become the development trend of passenger transport in various countries and regions. One of the most important components of a high-speed railway is pantograph-catenary system, which can provide electric power. When the pantograph slides on the contact wire, arc ablation will damage the pantograph material due to contact wire irregularity, vibration of pantograph head, fluctuation of contact net and other factors. The damage of pantograph material caused by arc erosion restricts the development of high-speed trains [1-5], which has drawn increasing attention in multidisciplinary field.

Due to good toughness, corrosion resistance [6], excellent electrical conductivity and thermal conductivity, copper is expected to be used as a pantograph cannot material. However, the strength of copper usually cannot meet the application requirements, and the problem can be solved by adding a reinforcement phase that does not affect conductivity seriously [7]. Zhang [8] investigated the cathode spot movement on the carbon fiber reinforced Cu matrix composite, and found that the cathode spot moves parallel to the carbon fibers, macroscopically. Wei [9] et al calculated the work function of W-Cu material. They found that the first vacuum breakdown probably occurs in the Cu phase, which was confirmed by Chen et al[10] through the analysis of the orientation distribution function (ODF). Dong et al[11] investigated that graphene can enhance the dielectric strength obviously. Yang et al[12] discovered that the CuW alloy with additive Zr exhibits a lower chopping current. Zhu et al[13] found that the

Received date: January 11, 2019
Foundation item: Natural Science Foundation of Anhui Province (1908085QE218, 1808085ME122); National Natural Science Foundation of China (51871085, 21503004)
Corresponding author: Feng Yi, Ph. D., Professor, School of Materials Science and Engineering, Hefei University of Technology, Hefei 230009, P. R. China, Tel: 0086-551-62904715, E-mail: fyhfut@163.com

arc life and arc energy of Cu/Cr20 follow a linear relationship. Zhang [14] et al confirmed that the W can improve the arc erosion properties of Al_2O_3-Cu electrical contacts.

In recent years, layered ternary compounds *MAX* phases (*M* stands for Ti, Sc, V, Cr, etc, *A* stands for Al, Si, Ga, Ge, etc, and *X* stands for C, N) are receiving more and more attention for their unique properties of ceramics and metals. *MAX* has good ceramic properties: high oxidation resistance, high temperature strength and low thermal expansion coefficient. *MAX* can also exhibit characteristics of metals, such as excellent thermal and electrical conductivity [15, 16]. A typical member of *MAX* phase is Ti_3AlC_2, whose thermal conductivity and electric conductivity are 27.5 $W \cdot m^{-1} \cdot K^{-1}$ and 2.9×10^6 $S \cdot m^{-1}$, respectively. At 1400 ℃, the mass of Ti_3AlC_2 only increases to 3.5×10^{-2} kg/m^2 after 20 h of oxidation. In addition, Ti_3AlC_2 exhibits high strength, thermal stability and low friction coefficient at high temperatures [17-20]. These particular properties make it a promising candidate for pantograph material and also an alternative reinforcement for Cu matrix.

Both *MAX* phase Ti_3AlC_2 and its composite Cu-Ti_3AlC_2 are candidate materials for pantograph system of high speed trains, but which one has better electrical ablation properties? Previous reports have unilaterally focused on the erosion performance of *MAX* phase materials and their composites. It was found that Ti_3SiC_2 cathode is decomposed into TiC_x under the vacuum arc [21, 22], due to the formation of a 5~50 μm thick converted layer [23]. Xie [24] studied the arc erosion properties of Cu-Ti_3SiC_2 composite, and found that vacuum arc is more prone to damage Ti_3SiC_2 particles than to damage the Cu matrix. There are few reports about arc erosion behavior of both Ti_3AlC_2 and Cu-Ti_3AlC_2 material. Here the eroded surfaces, arc morphologies at real time, arc life, breakdown voltage, arc energy, and composition of eroded Ti_3AlC_2 and Cu-Ti_3AlC_2 were compared systematically, which will provide scientific basis for selection of pantograph material.

1 Experiment

The Ti_3AlC_2 cathode was fabricated by suppressing-sintering-repressing technique. The initial materials were Ti_3AlC_2 powder with >98% purity, produced by pressureless calcining (PC) technique [25]. The steel die with Ti_3AlC_2 powder was first suppressed on a pressure machine (769YP-60A) under 300 MPa. The corundum canoe with preformed embryo body was put into the tube furnace (GSL-1600X) for sintering in a flowing argon atmosphere at 1300 ℃. The heating rate was 10 ℃/min. The holding time was 1 h, then cooling in the furnace. Subsequently, the sintered sample was placed back in the steel die for repressing at 500 MPa. After being removed from the steel die, the sintered sample was polished by several abrasive papers (240-, 400-, and 800-mesh). For removing surface contaminants, the polished sample was cleaned in an ultrasonic cleaning instrument with acetone solution, alcohol solution, and distilled water for 30 min. The phase composition of polished sample is shown in Fig.1a. It can be seen that the main phase is Ti_3AlC_2, with tiny Ti-Al intermetallic compounds and Al_2O_3 impurities. The insets in Fig.1 are secondary electron images of Ti_3AlC_2 surface, which is smooth without scratch left during the polishing process.

Copper powder (99.5%, 45 μm, Beijing Research Institute of Nonferrous Metals) and Ti_3AlC_2 powder (99.2%, ~5 μm) were used as the raw materials for Cu-Ti_3AlC_2 composite, which was prepared by the hot-pressing (HP) technique (ZT-40-20Y). The uniformly mixed Cu and Ti_3AlC_2 powders were put into graphite mould coated with boron nitride. Subsequently, the graphite mould was compressed at 30 MPa and heated to 800 ℃. After holding in an Ar atmosphere for 1 h, the material was cooled down in the furnace. The sintered Cu-Ti_3AlC_2 composite was also polished by abrasive papers as mentioned above. The phase composition is shown in Fig.1b. Only peaks of Cu and Ti_3AlC_2 phase were detected, indicating that no chemical reaction between Cu and Ti_3AlC_2 happens during the sintering process. The white arrows in the inset refer to Ti_3AlC_2, distributed uniformly in the Cu matrix.

Tungsten (>99%) was used as the anode, which was machined into a tip with 2 mm in diameter. Except W, no other

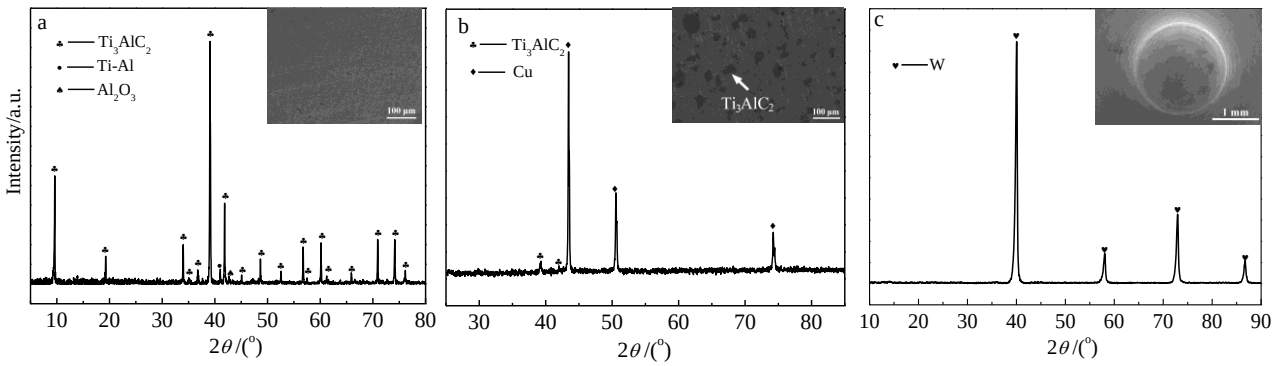

Fig.1 X-ray diffraction patterns and SEM images (insets) of sintered Ti_3AlC_2 (a), sintered Cu-Ti_3AlC_2 (b) and W anode (c)

impurity was detected in Fig.1c. The condition of tip surface is shown in the inset of Fig.1c. The surface is smooth without any tiny bulges, which may affect the accuracy of arc parameters.

The arc discharge operation of Ti_3AlC_2 or Cu-Ti_3AlC_2 material was carried out on a self-made arc erosion device, which is schematically shown in Fig.2. The polished Ti_3AlC_2 or Cu-Ti_3AlC_2 sample was set as the cathode, and the W anode was located below the cathode. The capacitor was used to charge the sample at different voltages (2~10 kV). The arc life, voltage and current as a function of time were analyzed by a digital memory oscilloscope (ADS1102CAL). The relative motion between the cathode and the anode was controlled by a stepper at a velocity of 0.2 mm/min. The arc shape and color were observed by a high-speed camera in real time (VW-9000, 12 000 frames/s). The X-ray spectroscopy with Cu Kα radiation (XRD, X'pert PRO MPD, 40 kV and 40 mA) was employed to analyze phases of the cathode and the anode. Analyses of the eroded morphology and elements distribution were conducted by a field-emission scanning electron microscope (FE-SEM, JEM-2100F), equipped with an energy-dispersive X-ray spectroscopy (EDS) apparatus. Raman spectroscopy (LabRAM-HR, Nd: YAG laser, 4 mW) was used to detect and analyze the products of the eroded sample over a wavenumber range of 100~1000 cm^{-1}.

2 Results and Discussion

Fig.3a~3d and Fig.3e~3h are the current-time curves of Ti_3AlC_2 and Cu-20 vol% Ti_3AlC_2 materials at the voltage of 2, 5, 7, and 9 kV, respectively. In the initial stage, the cathode moves to the W anode slowly before the air is conducted by the high voltage. During this stage, there is no current detected on the oscilloscope. If the arc forms between the two electrodes, the current increases rapidly to a certain value on the current-time curves. This certain value is called "breakdown current". For both Ti_3AlC_2 and Cu-Ti_3AlC_2 materials, the breakdown current increases with the erosion voltages. In order to compare the differences of breakdown currents at different voltages between the two materials more clearly, the data are shown in Table 1. It can be seen obviously that the breakdown current of Ti_3AlC_2 increases from 10.8 A to 58.3 A, and that of Cu-Ti_3AlC_2 increases from 10.4 A to 51.8 A. It is worth noting that at the same voltage, the breakdown current of Ti_3AlC_2 is higher than that of Cu-Ti_3AlC_2, meaning that the arc energy of Ti_3AlC_2 arc is higher than that of Cu-Ti_3AlC_2. The arc lives of Ti_3AlC_2 and Cu-Ti_3AlC_2 are labeled as blue and red fonts and arrows in Fig.3, respectively. Comparing Fig.3a and Fig.3e, it can be seen that the arc life of pure Ti_3AlC_2 material is about 5 ms higher than that of Cu-Ti_3AlC_2. The similar condition also happens at the voltage of 5, 7, and 9 kV.

The images for the whole discharge process of Ti_3AlC_2 and Cu-Ti_3AlC_2 recorded by high-speed camera are displayed in Fig.4. Both discharge processes contain three stages: arc formation, steady combustion and attenuation. Obviously, the arc column is focused on a certain point of the Ti_3AlC_2 cathode surface, while the arc column covers the whole surface of Cu-Ti_3AlC_2, meaning that the erosion depth of Ti_3AlC_2 is much deeper than that of Cu-Ti_3AlC_2. It can be seen that a large amount of droplet splashes appear in Fig.4b_1. No droplet splashes are observed on the arc morphologies of Cu-Ti_3AlC_2 from Fig.4a_2 to Fig.4h_2. The arc morphologies of the two materials indicate that the erosion degree of Ti_3AlC_2 is more serious than that of Cu-Ti_3AlC_2.

Field-emission scanning electron microscope was used to record the differences of eroded surface between Ti_3AlC_2 and Cu-Ti_3AlC_2, as presented in Fig.5 and Fig.6, respectively. For Ti_3AlC_2, microcracks are formed on the eroded surface at the voltage of 2, 5, 7, and 9 kV. Herein, only surface eroded at 9 kV is displayed due to the similar morphology. The eroded area is about 0.26 mm^2. It can be seen that there are holes in

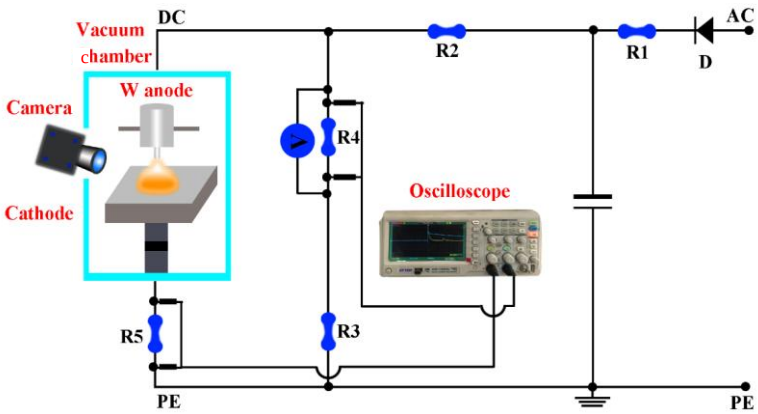

Fig.2 Schematic diagram of experimental arc ablation device

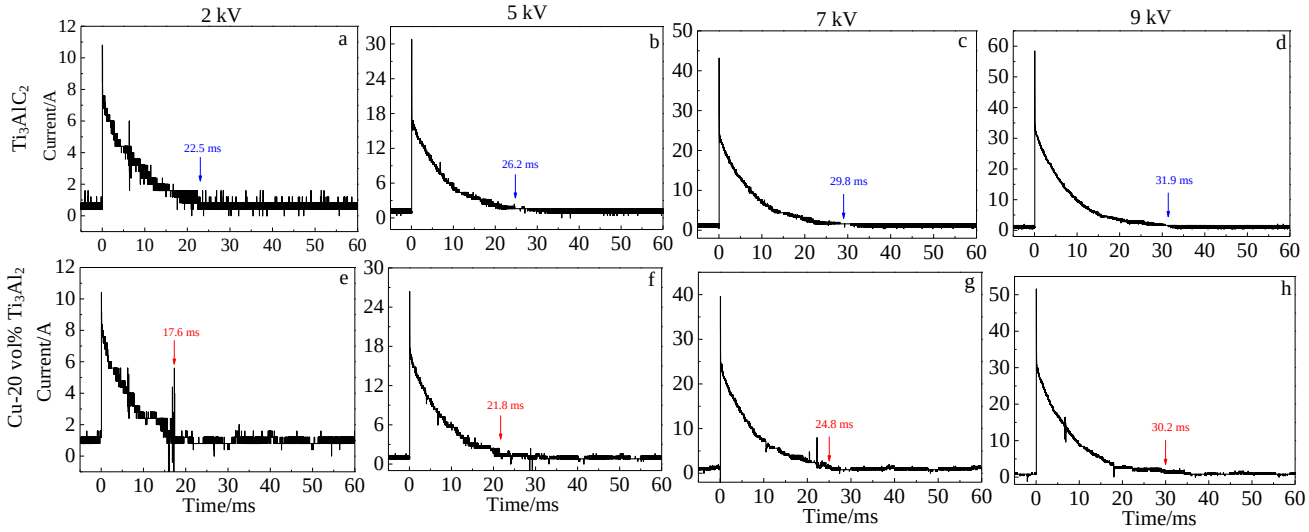

Fig.3 Current-time curves of Ti_3AlC_2 (a~d) and Cu-20 vol% Ti_3AlC_2 (e~h) under 2, 5, 7 and 9 kV

Table 1 Breakdown current of pure Ti_3AlC_2 and Cu-Ti_3AlC_2

Voltage/kV	Ti_3AlC_2 current/A	Cu-Ti_3AlC_2 current/A
9	58.3	51.8
7	43.2	39.8
5	30.8	26.1
2	10.8	10.4

the centre of eroded surface, surrounded by an irregular circle. The area inside circle is called “hot-melt zone”, labeled by red color. The area corresponds to the arc centre, where the energy and heat are the highest. The most peripheral area is called “droplet splash zone”, labeled by blue color, which refers to the arc edge. The yellow area between the “hot-melt zone” and the “droplet splash zone” is the “heat affected zone”. In the “heat affected zone”, the material melts and re-solidifies to “isolated island”, as shown in Fig.5b. The magnified microcrack is stretched to the whole surface, as shown in Fig.5d. In the “droplet splash zone”, the surface is covered with small spheres, shown in Fig.5c. The spheres with a diameter of about 2 μm are formed during the steady burning process in Fig.4. In this process, the molten material, together with air rolls around. After the arc is extinguished, the material cools down and the air exits, and finally, the morphologies in Fig.5f and Fig.5c are left behind. The hole in Fig.5e demonstrates that the eroded depth is deeper than that of Cu-Ti_3AlC_2, qualitatively.

Cu-Ti_3AlC_2 with four components (Ti_3AlC_2 content: 15 vol%, 20 vol%, 35 vol% and 40 vol%) was eroded at the voltage of 9 kV, shown in Fig.6, whose eroded areas are about 0.14, 1.00, 1.57 and 1.22 mm^2, respectively. The erosion area increases with increasing the Ti_3AlC_2 content. What’s more, the three zones mentioned above on the eroded Ti_3AlC_2 surface are not obvious on the Cu-Ti_3AlC_2 surface. In Fig.6e and Fig.6f, no microcrack is found. Only some droplets are solidified on the surface. The number of droplet is less than that of Ti_3AlC_2 in Fig.5c. When Ti_3AlC_2 content increases to 30 vol% and 40 vol%, microcrack forms on the eroded surface. No matter what the composition of Cu-Ti_3AlC_2 is, no obvious holes are discovered on the eroded Cu-Ti_3AlC_2 surfaces in Fig.6, demonstrating that the erosion degree is not as serious as that of pure Ti_3AlC_2 eroded at the same voltage.

The current-time curves of Cu-Ti_3AlC_2 with different Ti_3AlC_2 contents are shown in Fig.7. Combining the result in Fig.3h, it can be seen that all the breakdown currents of Cu-Ti_3AlC_2 with different Ti_3AlC_2 contents are about 50 A, which is less affected by the content of Ti_3AlC_2. The breakdown currents of Cu-Ti_3AlC_2 are less than that of Ti_3AlC_2 under the same voltage (58.3 A in Table 1).

For a given environmental medium, the arc energy can be calculated by the following Eq.(1)[26]:

$$E=UIt \quad (1)$$

where E is arc energy (J), U is arc voltage (V), I is breakdown current (A), and t is arc life (s). According to the breakdown currents of Cu-Ti_3AlC_2 and Ti_3AlC_2 materials at the voltage of 9 kV in Table 1 and the arc lives in Fig.3, the calculated arc energy is shown in Table 2. From Table 2, it can be seen that the arc energy of Ti_3AlC_2 material is larger than that of Cu-Ti_3AlC_2 material at the same voltage. The higher the arc energy, the more serious the damage to the electric contact material, which well explains the morphologies in Fig.5 and Fig.6.

The compositions of eroded Ti_3AlC_2 and Cu-Ti_3AlC_2 and their corresponding W anode after erosion at 9 kV were analyzed by EDS, as displayed in Fig.8. For eroded Ti_3AlC_2 in Fig.8a, O, Ti, Al and W elements are detected. The W element arises from W anode, meaning that during the process of arc combustion, W anode is also sputtered onto

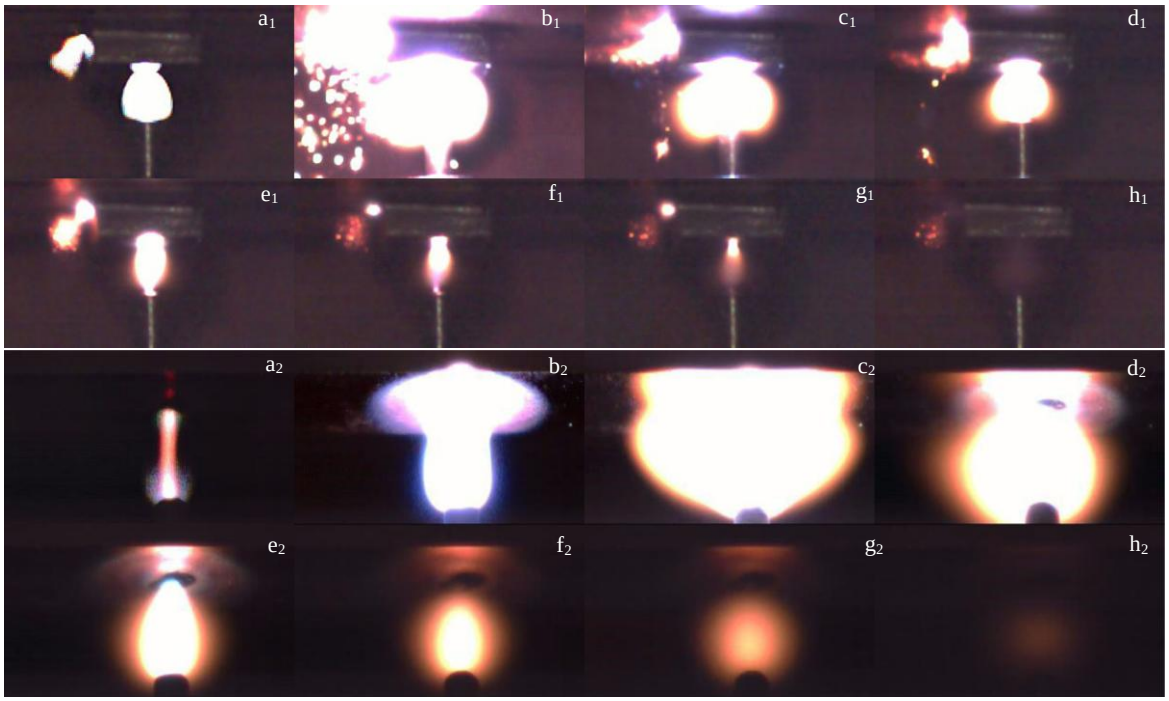

Fig.4 Arc morphology of Ti_3AlC_2 (a_1~h_1) and Cu-Ti_3AlC_2 (a_2~h_2) during the whole discharge process: (a_1, a_2) arc formation, (b_1~d_1, b_2~d_2) steady combustion, and (e_1~h_1, e_2~h_2) attenuation

the Ti_3AlC_2 surface. The atomic percentage of Ti and Al element is 22.4% and 13.0%, respectively. If Ti and Al elements are oxidized totally, the calculation result (O%=Ti%×2+Al%×1.5) of O element should be 64.3%. The calculation result accords with the EDS result (64.1%) of O element in Fig.8a, indicating that Ti_3AlC_2 material is decomposed and oxidized by arc erosion. In Fig.8b, the ratio of O and W element is 1.59, meaning that part of W element is oxidized to tungsten oxide. For Cu-Ti_3AlC_2 surface, if Cu, Ti and Al elements are oxidized totally, the calculation result (O%=Cu%×1+Ti%×2+Al%×1.5) of O element should be 52.7%. The result is also approximately equal to the detected value (52.5%), demonstrating that Cu-Ti_3AlC_2 material is also decomposed and oxidized after erosion by electric arc. It is worth noting that except for W and O, Cu element is also detected on the W anode in Fig.8d, which derives from corresponding Cu-Ti_3AlC_2 cathode.

Raman spectrum is considered a useful tool for analyzing the material composition. The advantage of Raman spectroscopy is that the interesting region can be selected under an optical microscope. To further confirm the composition of the erosion product, the eroded surfaces of Ti_3AlC_2 and

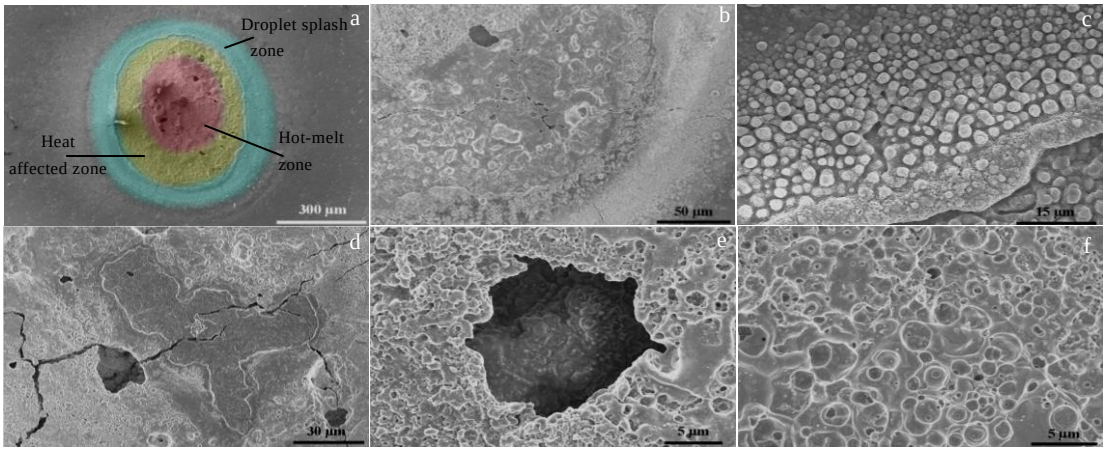

Fig.5 Eroded morphologies of Ti_3AlC_2 at 9 kV: (a) three zones, (b) isolated island, (c) small spheres, (d) crack, and (e, f) holes

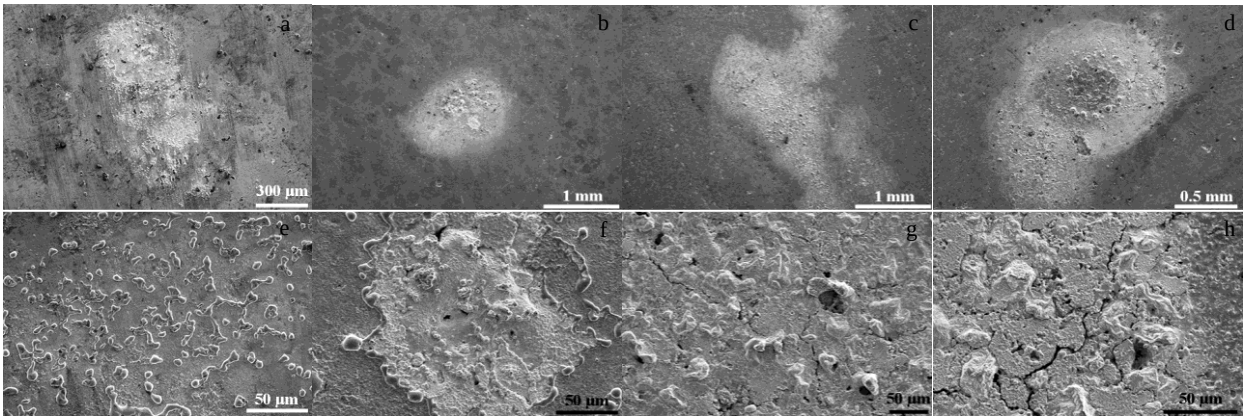

Fig.6 Eroded morphologies of Cu-Ti_3AlC_2 with different Ti_3AlC_2 contents: (a, e) 15 vol%, (b, f) 20 vol%, (c, g) 35 vol%, and (d, h) 40 vol%

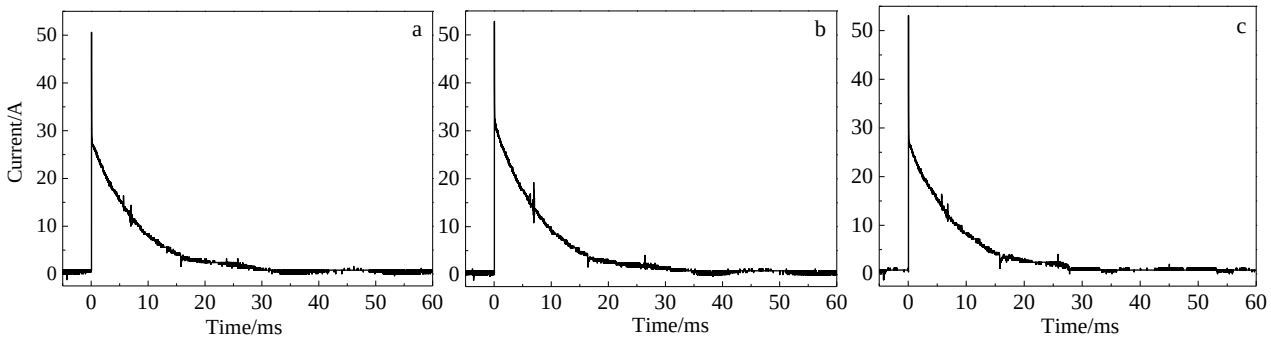

Fig.7 Current-time curves of Cu-15 vol% Ti_3AlC_2 (a), Cu-35 vol% Ti_3AlC_2 (b), and Cu-40 vol% Ti_3AlC_2 (c) at 9 kV

Table 2 Arc energy of Ti_3AlC_2 and Cu-20 vol% Ti_3AlC_2 material at 2, 5, 7, and 9 kV

Voltage/kV	2	5	7	9
Arc energy of Ti_3AlC_2/J	486	4034.8	9011.52	16737.93
Arc energy of Cu-20 vol% Ti_3AlC_2/J	366.08	2844.9	6909.28	14079.24

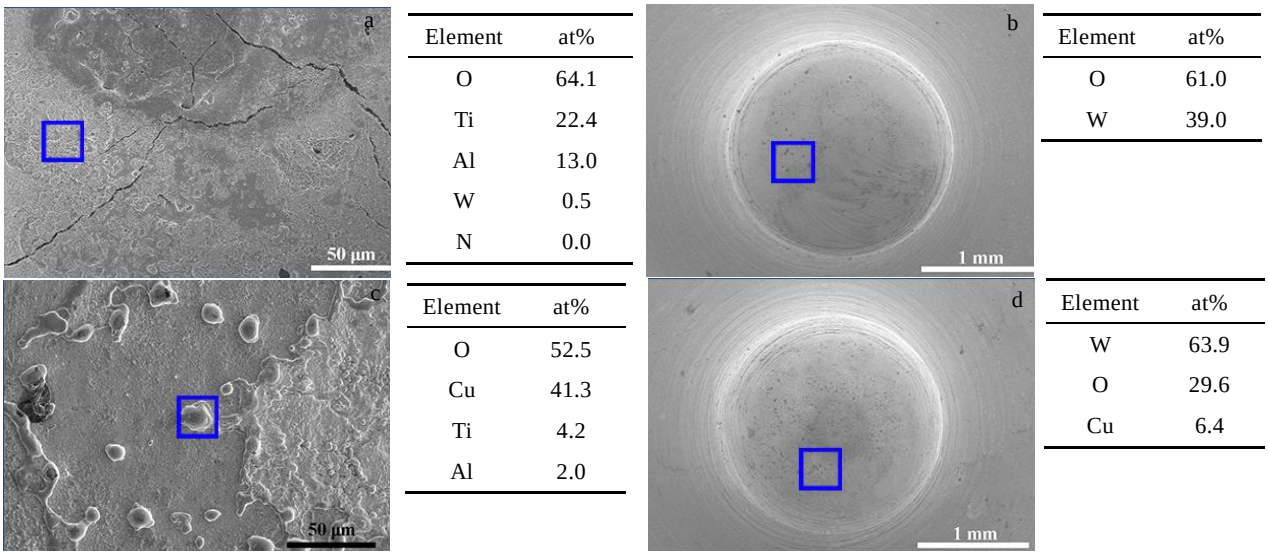

Element	at%
O	64.1
Ti	22.4
Al	13.0
W	0.5
N	0.0

Element	at%
O	61.0
W	39.0

Element	at%
O	52.5
Cu	41.3
Ti	4.2
Al	2.0

Element	at%
W	63.9
O	29.6
Cu	6.4

Fig.8 EDS results of eroded Ti_3AlC_2 (a) and corresponding W anode (b), and Cu-Ti_3AlC_2 (c) and corresponding W anode (d)

Cu-Ti_3AlC_2 are analyzed by Raman spectroscopy, as shown in Fig.9a and Fig.9b, respectively. The laser is conducted at the green cross. In Fig.9a, shift of TiO_2 (211, 315 cm^{-1}) and Al_2O_3 (579 cm^{-1}) appears [27-29], which confirms the EDS result in Fig.8a. In Fig.9b, besides shifts of TiO_2 (153, 279, 610 cm^{-1}) and Al_2O_3 (382 cm^{-1}), peaks at 820 916 cm^{-1} correspond to CuO (R060978). Cu-Ti_3AlC_2 is also decomposed and oxidized, which is in agreement with the EDS result in Fig.8b.

The process of arc combustion is to some extent an electric and thermal phenomenon. If the processes of arc heat dissipation and the energy consumption last for a shorter period of time, the process of arc column de-dissociation will be stronger and the arc life will be shorter. It is favorable to prolong the service life of an electric contact material [30]. The oxidation process is actually the process of arc energy consumption. More kinds and quantities of oxide formation consume more energy. In this condition, the arc is extinct rapidly. Comparing the products on eroded Ti_3AlC_2 and Cu-Ti_3AlC_2, it can be seen that apart from TiO_2 and Al_2O_3, CuO is also formed on the Cu-Ti_3AlC_2 surface. That is to say, the arc consumption of Cu-Ti_3AlC_2 is faster, which well explains the results in Fig.3. What's more, previous studies have shown that the addition of a single metal oxide in electric contact materials can effectively improve the wettability between the matrix material and the oxide, and reduce the droplet splashes and mass loss of a cathode material [31-37]. It can be inferred that the materials with multiple oxides have better wettability and less splashes, which needs further systematical and deep study in the future.

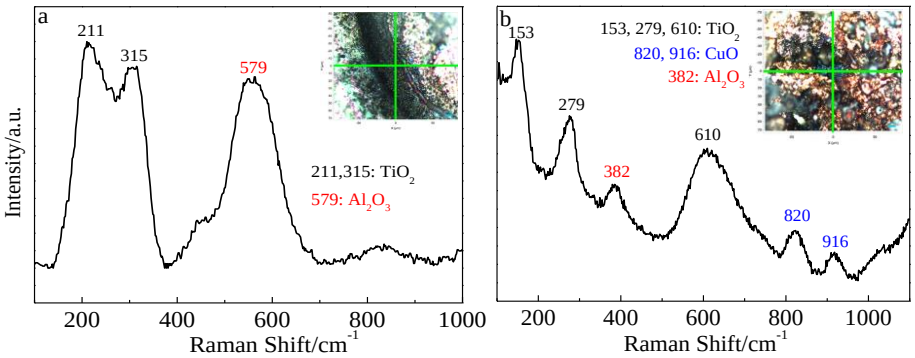

Fig.9 Raman spectra of eroded Ti_3AlC_2 (a) and Cu-Ti_3AlC_2 (b)

3 Conclusions

1) The electric arc of Cu-Ti_3AlC_2 is more dispersed than that of Ti_3AlC_2, which meets the performance requirement that the electric arc can be widely dispersed on the material.

2) The arc life and breakdown current of Cu-Ti_3AlC_2 are smaller than those of Ti_3AlC_2, and the arc energy of Cu-Ti_3AlC_2 material is less than that of Ti_3AlC_2 material under the same voltage. Because the electric materials should have shorter arc life and smaller breakdown current, Cu-Ti_3AlC_2 is better than Ti_3AlC_2 to be a kind of pantograph material.

3) The eroded Ti_3AlC_2 surface is more uneven, covered with "holes", "microcracks", and "droplet splashes". No microcrack is generated on the surface of Cu-Ti_3AlC_2 with Ti_3AlC_2 less than 30 vol%. Furthermore, the number of "holes" and "droplet splashes" is less than that of the pure Ti_3AlC_2, demonstrating that the eroded Cu-Ti_3AlC_2 has a more even surface, which meets the performance requirement of electric materials that should have a more smooth eroded material surface.

References

1 Vo Van O, Massat J-P, Balmes E. *Journal of Sound and Vibration*[J], 2017, 402: 51

2 Ren Wanbin, Wang Tengyu, Zhang Xu *et al*. *IEEE Transactions on Components, Packaging and Manufacturing Technology*[J], 2019, 9: 18

3 Wu Chunping, Yi Danqing, Weng Wei *et al*. *Materials & Design*[J], 2015, 85: 511

4 Wang Xianhui, Yang Hao, Liang Shuhua *et al*. *Rare Metal Materials and Engineering*[J], 2015, 44(11): 2612

5 Wang Haitao, Wang Jingqin, Du Jiang *et al*. *Rare Metal Materials and Engineering*[J], 2014, 43(8): 1846

6 Meng Linglong, Wang Xiaojun, Hu Xiaoshi *et al*. *Composites Part A: Applied Science and Manufacturing*[J], 2019, 116: 138

7 Qian Gang, Feng Yi, Chen Fanyan *et al*. *Science China Technological Sciences*[J], 2013, 56: 2839

8 Zhang Chengyu, Liu Yiwen, Yang Zhimao *et al*. *Vacuum*[J], 2013, 93: 45

9 Wei Xin, Yu Demei, Sun Zhanbo *et al*. *Vacuum*[J], 2014, 107: 83

10 Chen Qiuyu, Liang Shuhua, Wang Feng *et al*. *Vacuum*[J], 2018, 149: 256

11 Dong longlong, Chen Wenge, Deng Nan *et al*. *Journal of Al-*

loys and Compounds[J], 2017, 696: 923
12 Yang Xiaohong, Zou Juntao, Xiao Peng *et al*. *Vacuum*[J], 2014, 106: 16
13 Zhu Shunxin, Liu Yong, Tian Baohong *et al*. *Vacuum*[J], 2017, 143: 129
14 Zhang Xiaohui, Zhang Yi, Tian Baohong *et al*. *Composites Part B*[J], 2019, 160: 110
15 Barsoum M W. *Progress in Solid State Chemistry*[J], 2000, 28: 201
16 Wang Zhiquan, Zhong Zhihong, Sun Bowen *et al*. *Materials Science and Engineering A*[J], 2019, 742: 169
17 Sun Zhengming. *International Materials Reviews*[J], 2001, 56(3): 143
18 Radovic M, Barsoum M W. *American Ceramic Society Bulletin*[J], 2013, 92: 20
19 Tzenov N V, Barsoum, M W. *Journal of the American Ceramic Society*[J], 2010, 83: 825
20 Singh B K, Ghosh K, Roy S S *et al*. *Transactions of the Indian Ceramic Society*[J], 2018, 77(4): 219
21 Zhang Peng, Ngai T L, Xie, Heng *et al*. *Journal of Physics D: Applied Physics*[J], 2013, 46: 395 202
22 Zhang Peng, Ngai T L, Xie Heng *et al*. *Physics Letters A*[J], 2014, 378(32-33): 2417
23 Zhu Jiqi, Eriksson A O, Ghafoor N. *Journal of Vacuum Science & Technology A*[J], 2011, 29: 31 601
24 Xie Heng, Ngai T L, Zhang Peng *et al*. *Vacuum*[J], 2015, 114: 26
25 Kubo Shunichi, Kato Koji. *Tribology International*[J], 1999, 32: 367
26 Tang Hai, Feng Yi, Huang Xiaochen *et al*. *Rare Metal Materials and Engineering*[J], 2017, 46(8): 2108
27 Porto S P S, Krishnan R S. *Journal of Chemical Physics*[J], 1967, 47: 1009
28 Parker J C, Siegel R W. *Applied Physics Letters*[J], 1990, 57: 943
29 Swamy V. *Physical Review B*[J], 2008, 77: 998
30 Farrall G A, Cobine J D. *Journal of Applied Physics*[J], 1965, 36(1): 53
31 Wei Zhijun, Zhang Lingjie, Yang Hui *et al*. *Journal of Materials Research*[J], 2016, 31: 468
32 Wei Zhijun, Zhang Lingjie, Shen Tao *et al*. *Journal of Materials Engineering and Performance*[J], 2016, 25: 3662
33 Wang Jun, Kang Yongqiang, Wang Chen. *Journal of Alloys and Compounds*[J], 2016, 686: 702
34 Li Guijing, Cui Huijie, Chen Jun *et al*. *Journal of Alloys and Compounds*[J], 2017, 696: 1228
35 Li Hangyu, Wang Xianhui, Xi Yong *et al*. *Materials & Design*[J], 2017, 121: 85
36 Wang Jun, Kang Yongqiang, Wang Chen *et al*. *Journal of Alloys and Compounds*[J], 2018, 756: 202
37 Wang Jun, Zhao Haidong, Wang Junbo *et al*. *Journal of Alloys and Compounds*[J], 2019, 770: 920

受电弓材料 Ti_3AlC_2 和 Cu-Ti_3AlC_2 的电弧烧蚀性能对比

黄晓晨[1]，凤 仪[2]，钱 刚[2]，葛金龙[1]，张现峰[1]，王传虎[1]
(1. 蚌埠学院 硅基新材料工程技术研究中心，安徽 蚌埠 233030)
(2. 合肥工业大学，安徽 合肥 230009)

摘 要：经过 2, 5, 7, 9 kV 放电电压作用后，分析了受电弓材料 Ti_3AlC_2 和 Cu-Ti_3AlC_2 的电弧烧蚀性。Cu-Ti_3AlC_2 材料的电弧寿命和击穿电流都比 Ti_3AlC_2 的低。用高速摄影机记录 2 种材料的电弧形态。结果表明，Ti_3AlC_2 上的电弧要比 Cu-Ti_3AlC_2 的电弧更加集中，伴随着更多的液滴飞溅。采用扫描电镜（SEM）观察了被侵蚀的 2 种材料表面情况。和 Cu-Ti_3AlC_2 的表面相比，Ti_3AlC_2 的表面更加不均匀，表面覆盖有“孔洞”，“显微裂纹”和“飞溅物”。计算了不同电压下的电弧能量，在相同电压下，Cu-Ti_3AlC_2 材料的电弧能量小于 Ti_3AlC_2 材料。采用拉曼光谱法测定了被烧损样品表面的成分。实验表明，Cu-Ti_3AlC_2 更适合于做受电弓材料。

关键词：Ti_3AlC_2；Cu-Ti_3AlC_2；电弧侵蚀；高速摄影机

作者简介：黄晓晨，女，1989 年生，博士，讲师，蚌埠学院硅基新材料工程技术研究中心，安徽 蚌埠 233030，电话：0552-3179368，E-mail: xiaochenhuang@yeah.net